Inorg. Chem. **2008**, *47*, 5882−5888

Biomolecule-Assisted Synthesis of Water-Soluble Silver Nanoparticles and Their Biomedical Applications

Qingzhi Wu,[†] Huaqiang Cao,*[,†,§] Qiuying Luan,[‡] Jiyong Zhang,[‡] Zhao Wang,*[,‡] Jamie H. Warner,[§] and Andrew A. R. Watt[§]

Department of Chemistry, Tsinghua University, Beijing 100084, P. R. China, School of Medicine, Tsinghua University, Beijing 100084, P. R. China, and Department of Materials, Oxford University, Oxford OX1 3PH, U.K.

Received February 3, 2008

The application of nanoparticles in the biomedical field is an exciting interdisciplinary research area in current materials science. In the present study, size-tunable and water-soluble noble metal silver nanoparticles (Ag NPs) have been successfully synthesized with the assistance of glutathione (GSH). The as-synthesized Ag NPs are ready to bind covalently with a model protein (bovine serum albumin) in mild conditions. The optical property of surface-modifiable Ag NPs was extremely sensitive to their size and the surface modification, suggesting a potential in the biomedical analysis and detection. Furthermore, Ag NPs with an average diameter of ca. 6 nm effectively suppress the proliferation of human leukemic K562 cells in the dose- and time-dependent manners, suggesting the promising potential of Ag NPs in cancer therapy.

1. Introduction

Nanotechnology applied to biomedical fields has become one of the most important and challenging focuses in the past decades. Functionalized, inert, and biocompatible nanomaterials have attracted considerable attention due to their potential applications in biomedical analysis, especially in cancer diagnosis and therapy.[1−4] For instance, nanovectors have been used in the targeted delivery of anticancer drugs and as imaging contrast agents.[2] Research in fluorescent and magnetic nanocrystals has been concentrated on the detection and monitoring of tumor biomarkers.[3] Also, nanocrystals have been utilized in the hyperthermia and photodynamic therapy of malignant tumors.[4] However, imparting the nanocrystals with target-recognizing, water-soluble, and precise biomedical functions through the surface modification still needs much more effort.

Noble metal silver (Ag) and Ag salts have been used as powerful antimicrobial agents for many years.[5] Recently, Ag nanoparticles (NPs) have attracted a great deal of attention in biomedical applications derived from its surface plasmon resonance effect and antibacterial activity. Interaction of single Ag NPs with light is the most efficient among the same dimensional particles composed of other organic or inorganic chromophores.[6] Ag NPs have therefore been applied as the optical indicator for single-molecule detection in biological assays.[7] It has been reported that Ag NPs can act against Gram-negative bacteria[8] and exhibit cytoprotective activity toward HIV-1 infected cells.[9] Also, nanocrystal

* To whom correspondence should be addressed. E-mail: hqcao@mail.tsinghua.edu.cn or huaqiang.cao@materials.ox.ac.uk (H.C.), zwang@tsinghua.edu.cn (Z.W.).
† Department of Chemistry, Tsinghua University.
§ Department of Materials, Oxford University.
‡ School of Medicine, Tsinghua University.

(1) (a) Ferrari, M. *Nat. Rev. Cancer* **2005**, *5*, 161. (b) Brigger, I.; Dubernet, C.; Couvreur, P. *Adv. Drug Delivery Rev.* **2002**, *54*, 631. (c) Alivisatos, P. *Nat. Biotechnol.* **2004**, *22*, 47.
(2) Sengupta, S.; Eavarone, D.; Capila, I.; Zhao, G. L.; Watson, N.; Kiziltepe, T.; Sasisekharan, R. *Nature* **2005**, *436*, 568.
(3) (a) Gao, X. H.; Cui, Y. Y.; Levenson, R. M.; Chung, L. W. K.; Nie, S. M. *Nat. Biotechnol.* **2004**, *22*, 969. (b) Huh, Y. M.; Jun, Y. W.; Song, H. T.; Kim, S. J.; Choi, J. S.; Lee, J. H.; Yoon, S.; Kim, K. S.; Shin, J. S.; Suh, J. S.; Cheon, J. *J. Am. Chem. Soc.* **2005**, *127*, 12387.
(4) (a) Roy, I.; Ohulchanskyy, T. Y.; Pudavar, H. E.; Bergey, E. J.; Oseroff, A. R.; Morgan, J.; Dougherty, T. J.; Prasad, P. N. *J. Am. Chem. Soc.* **2003**, *125*, 7860. (b) Ivkov, R.; DeNardo, S. J.; Daum, W.; Foreman, A. R.; Goldstein, R. C.; Nemkov, V. S.; DeNardo, G. L. *Clin. Cancer Res.* **2005**, *11*, 7093.
(5) Gupta, A.; Silver, S. *Nat. Biotechnol.* **1998**, *16*, 888.
(6) Malynych, S.; Chumanov, G. *J. Am. Chem. Soc.* **2003**, *125*, 2896.
(7) Schultz, S.; Smith, D. R.; Mock, J. J.; Schultz, D. A. *Proc. Natl. Acad. Sci. U.S.A.* **2000**, *97*, 996.
(8) (a) Lee, H. Y.; Park, H. K.; Lee, Y. M.; Kim, K.; Park, S. B. *Chem. Commun.* **2007**, *28*, 2959. (b) Lok, C. N.; Ho, C. M.; Chen, R.; He, Q. Y.; Yu, W. Y.; Sun, H. Z.; Tam, P. K. H.; Chiu, J. F.; Che, C. M. *J. Biol. Inorg. Chem.* **2007**, *12*, 527.
(9) Sun, R. W. Y.; Chen, R.; Chung, N. P. Y.; Ho, C. M.; Lin, C. L. S.; Che, C. M. *Chem. Commun.* **2005**, *40*, 5059.

10.1021/ic8002228 CCC: $40.75
Published on Web 05/23/2008

Ag was reported to significantly augment the apoptosis of inflammatory cells in animal models, which facilitates the early phases of wound healing and inhibits allergic contact dermatitis.[10] Nevertheless, there have been few therapeutic applications of Ag NPs reported in the literature, especially in research on anticancer activity. Thus, there is still a large amount of development required in this promising field.

Inspired by the studies of biomineralization, biomolecules have been extensively utilized in the synthesis and assembly of nanomaterials.[11] Glutathione (GSH, γ-Glu-Cys-Gly-) plays a crucial role in protecting intracellular components against oxidative damage and detoxifying heavy metal ions through the mercapto group in an organism.[12] In particularly, GSH has two free $-$COOH groups and a $-NH_2$ group to provide a hydrophilic interface and a handle for further reactivity with other functional molecules. GSH is thus considered as an ideal capping molecule in the synthesis of metal and semiconductor nanocrystals, such as gold,[13] silver,[14] CdS and CdTe,[15] ZnSe[16] NPs, and so forth.

Herein, we report the synthesis of water-soluble and size-tunable Ag NPs using GSH as a capping agent. The as-synthesized Ag NPs are ready to bind with other functional molecules (bovine serum albumin, BSA, was used as a model protein in this report), and exhibit optical properties that are highly sensitive to changes in the particle size and surface modification. Furthermore, the stable and water-soluble Ag NPs, with an average diameter of ca. 6 nm, have been demonstrated to effectively inhibit the proliferation of human leukemic K562 cells in vitro. This implies that the Ag NPs are extremely promising as cancer therapeutic agents.

2. Experimental Section

2.1. Synthesis of GSH-coated Ag NPs. Ag NPs were synthesized according to a modified method.[14,17] Briefly, an aqueous solution of GSH (25×10^{-3} M) was added dropwise into an aqueous solution of silver nitrate (3×10^{-3} M) under vigorous stirring. The molar ratio between GSH and silver nitrate (GSH/$AgNO_3$) was adjusted from 1:1 to 1:2 and 1:10, respectively. After stirring for 15 min, the sodium borohydride aqueous solution (100×10^{-3} M) was rapidly added at a molar ratio of 8:1 between the reducing agent and silver nitrate under vigorous stirring. Immediately, the color of the solution turned from yellow to deep brown. The reaction was carried out in the absence of light and continued for 4 h at room temperature (16 ± 1 °C). The products were precipitated with absolute ethanol at a volume ratio of 4 and isolated by repeated centrifugation at 10 000 rpm for 5 min.

2.2. Characterization of Ag NPs. The phase identification of samples was performed by a Bruker D8 Advance Diffractometer (Cu Kα radiation, $\lambda = 1.5418$ Å). TEM images of the samples were obtained with a Hitachi-800 transmission electron microscope operating at 120 kV. The surface structures of the samples were characterized with a Nicolet 560 Fourier Transform infrared Spectrophotometer (FTIR). UV$-$vis absorption spectra were recorded at room temperature using a UV-2102 PC UV$-$vis spectrophotometer (UNICO Corp., China).

2.3. Ag NPs and BSA Binding. In a typical procedure, Ag NPs aqueous solution (4 mL) of a designed concentration was added into a 7 mL plastic tube, and BSA aqueous solution (2.5 mg/mL, 0.5 mL) and phosphate-buffered saline (PBS, 0.01 M, pH = 7.4, 0.4 mL) were added in turn. After the above solution was shaken for 15 min at room temperature (16 ± 1 °C), 100 μL of diluted glutaraldehyde aqueous solution (that was obtained by diluting 1.5 mL 25% glutaraldehyde solution into 10 mL) was added. The final concentration of Ag NPs was adjusted to 0.4, 0.6, 0.8, and 1.0 mg/mL, respectively. After another 5 min shaking, the above mixture was incubated at 37 °C for 1 h. After incubation, the mixture was stored at -20 °C. No subsequent treatment was adopted.

2.4. SDS-PAGE of Ag NPs and BSA Binding.[18] The sodium dodecyl sulfate polyacrylamide gel electrophoresis (SDS-PAGE) was carried out using a Bio-Rad electrophoresis system. A 50 μL sample was mixed with 10 μL of the sample buffer (50% glycerol, 10% SDS, 0.1% bromophenol blue, and Tris-HCl pH = 6.8). The sample mixture was denatured at 98 °C for 1.5 min (3 and 6 min denatured times were employed for studying the thermostability of binding products). A 10 μL sample mixture was loaded for the electrophoresis separation. The gel was stained with Comassie Blue after a suitable electrophoresis front was achieved.

2.5. Cell Culture and Treatment. The human leukemic K562 cell line was obtained from the Academy of Military Science of China, and cultured in RPMI 1640 medium supplemented with 10% fetal calf serum, 100 U/mL penicillin, 100 μg/mL streptomycin, and maintained at 37 °C in the air with mixture of 5% CO_2.

2.6. MTT (Thiazolyl Blue) Assay.[19] A 200 μL suspension of K562 cells per well was seeded in a 96-well plate at a density of 5×10^4 cells/mL. Cells grew for 12 h after seeding and were then treated with Ag NPs or GSH at the designed concentration (5, 10, 15, 20, and 25 μg/mL) for different times (6, 12, and 24 h). Cells were resuspended in a flash culture medium after a centrifugation at 1000 rpm for 10 min. Twenty microliters of MTT (5 mg/mL) was added to each well, and incubation was allowed to continue for a further 4 h. Finally, all media were removed by the centrifugation and 150 μL DMSO was added to each well and shaken for 10 min. The absorbance was read at a wavelength of 550 nm using a Benchmark Microplate Reader (Bio-Rad Corp. USA).

2.7. Fluorescence Observation of K562 Cells Stained by Hoechst 33258.[20] To distinguish living cells from apoptotic and necrotic cells, K562 cells were stained with fluorescent dye. A 2 mL suspension of K562 cells per well was seeded in a 12-well plate at a density of 1×10^5 cells/mL. Cells grew for 12 h after seeding, then were treated with Ag NPs or GSH at the designed concentration (5, 15, and 25 μg/mL) for different times (6, 12, and 24 h). After being washed with ice-cold PBS two times, cells were fixed with 200 μL methanol for 10 min at room temperature. Then,

(10) (a) Wright, J. B.; Lam, K.; Buret, A. G.; Olson, M. E.; Burrell, R. E. *Wound Rep. Reg.* **2002**, *10*, 141. (b) Bhol, K. C.; Schechter, P. J. *Br. J. Dermatol.* **2005**, *152*, 1235.
(11) Katz, E.; Willner, I. *Angew. Chem., Int. Ed.* **2004**, *43*, 6042.
(12) Mehra, R. K.; Tran, K.; Scott, G. W.; Mulchandani, P.; Saini, S. S. *J. Inorg. Biochem.* **1996**, *61*, 125.
(13) (a) Kou, X. S.; Zhang, S. Z.; Yang, Z.; Tsung, C. K.; Studky, G. D.; Sun, L. D.; Wang, J. F.; Yan, C. H. *J. Am. Chem. Soc.* **2007**, *129*, 6402. (b) Shichibu, Y.; Negishi, Y.; Tsunoyama, H.; Kanehara, M.; Teranishi, T.; Tsukuda, T. *Small* **2007**, *3*, 835.
(14) Slocik, J. M.; Wright, D. W. *Biomacromolecules* **2003**, *4*, 1135.
(15) (a) Barglik-Chory, C.; Remenyi, C.; Strohm, H.; Müller, G. *J. Phys. Chem. B* **2004**, *108*, 7637. (b) Qian, H. F.; Dong, C. Q.; Weng, J. F.; Ren, J. C. *Small* **2006**, *2*, 747.
(16) Zheng, Y. G.; Yang, Z. C.; Ying, J. Y. *Adv. Mater.* **2007**, *19*, 1475.
(17) Jiang, X. C.; Xie, Y.; Lu, J.; Zhu, L. Y.; He, W.; Qian, Y. T. *Langmuir* **2001**, *17*, 3795.
(18) Mamedova, N. N.; Kotov, N. A.; Rogach, A. L.; Studer, J. *Nano Lett.* **2001**, *1*, 281.
(19) Mosmann, T. *J. Immunol. Methods* **1983**, *65*, 55.
(20) Peng, L. M.; Wang, Z. L. *The Foundation and Clinic of Cell Apoptosis*; People's Medical Publishing House: Beijing, China, **2000**, 162.

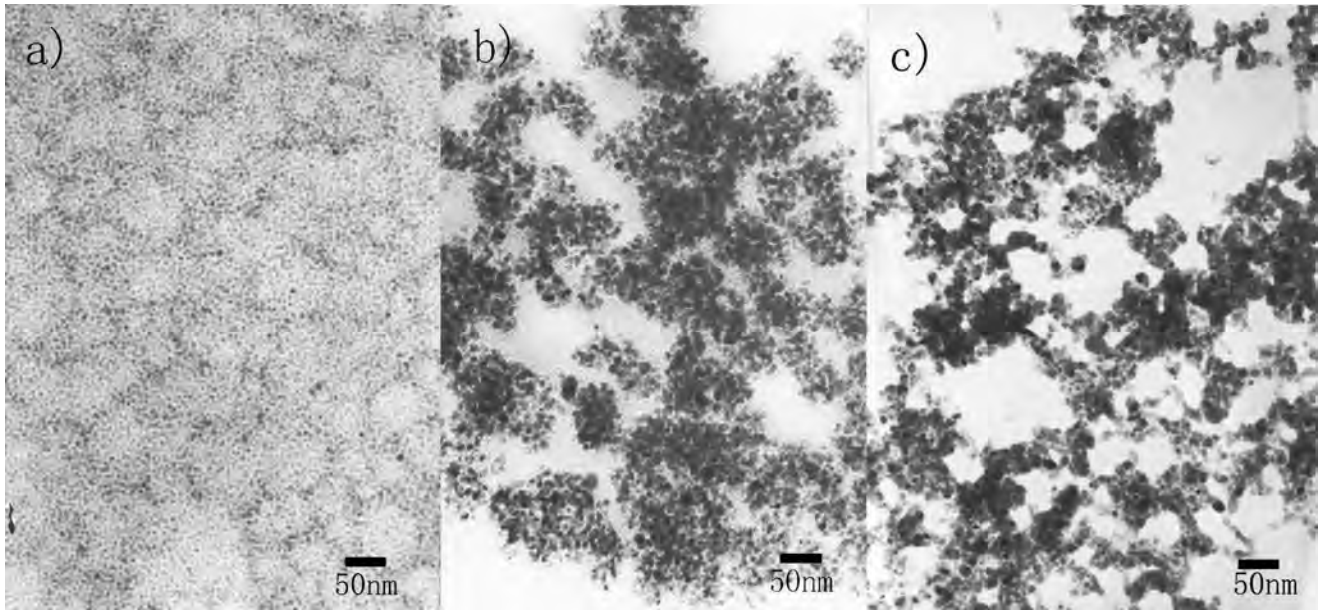

Figure 1. TEM images of Ag NPs synthesized at different GSH/$AgNO_3$ molar ratio; a) GSH/$AgNO_3$ molar ratio at 1:1, b) GSH/$AgNO_3$ molar ratio at 1:2, c) GSH/$AgNO_3$ molar ratio at 1:10.

cells were washed with PBS and resuspended in PBS, followed by adding 20 μL Hoechst 33258 (100 μg/mL) to a 80 μL cell suspension. Cells were stained at 37 °C for 10 min. Finally, cells were resuspended in 30 μL PBS after being washed with PBS through the centrifugation. A 20 μL cell suspension was spread on the glass scorer, observed, and pictures were taken using a DMIRB Inverted Fluorescence Microscope (Leica Corp., German).

2.8. Flow Cytometer Measurement. To assay the percentages of apoptosis and necrotic cells, FITC-annexin V and propidium iodide (PI)-stained cells were analyzed. A 2 mL suspension of K562 cells per well was seeded in a 12-well plate at a density of 8×10^4 cells/mL. Cells grew for 12 h after seeding and were then treated with Ag NPs or GSH at the designed concentration (5, 15, and 25 μg/mL) for different times (6, 12, and 24 h). After being washed with ice-cold PBS two times, cells were resuspended in 200 μL binding buffer (10 mM HEPES/NaOH, pH 7.4, 150 mM NaCl, 5 mM KCl, 1 mM $MgCl_2$, 1.8 mM $CaCl_2$) and coincubated with 10 μL FITC-annexin V (25 μg/mL) and 5 μL propidium iodide (PI, 50 μg/mL) in the absence of light for 15 min at room temperature. Finally, fluorescence intensities of cells stained were analyzed using a FACScalibur Flow cytometer (Becton Dickinson Corp., USA).

3. Results and Discussion

3.1. Ag NPs and Structures. Figure 1 shows the typical transmission electron microscopy (TEM) images of three samples synthesized with different reactant molar ratios (GSH/$AgNO_3$). The size of the particles could be tuned by adjusting the GSH/$AgNO_3$ molar ratio. When the GSH/$AgNO_3$ molar ratio was changed from 1:1 to 1:2 and then 1:10, the average particle sizes obtained from the TEM images were ca. 6, 8, and 11 nm, corresponding to parts a−c of Figure 1, respectively. As shown in parts a−c of Figure 1, minimal aggregation was observed when the GSH concentration was increased in the synthesis process. We speculate that this is due to the relatively high adsorption of GSH molecules onto the particle surfaces.

The crystalline phase of the as-synthesized samples was identified by X-ray diffraction (XRD). The (111), (200),

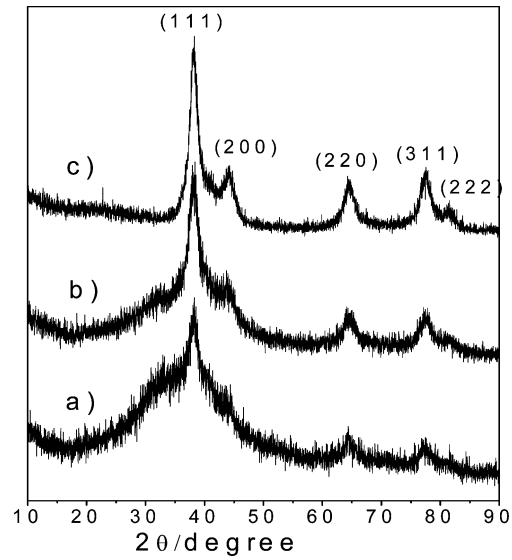

Figure 2. XRD patterns of Ag NPs synthesized at different GSH/$AgNO_3$ molar ratio; a) GSH/$AgNO_3$ molar ratio at 1:1, b) GSH/$AgNO_3$ molar ratio at 1:2, c) GSH/$AgNO_3$ molar ratio at 1:10.

(220), (311), and (222) plane shown in Figure 2 can be indexed to the cubic structure of silver (JCPDS 4−783). No peaks related to other crystalline phases were found. However, in part a of Figure 2 the (111) peak is significantly broadened along with the (200) peak not be observed. This is ascribed to a decrease in the particle size derived from the change in the GSH/$AgNO_3$ molar ratio. This result is consistent with the TEM observation as shown in Figure 1.

Detail information about the surface of the as-synthesized Ag NPs can be obtained from infrared spectroscopy (Figure 3). A sharp peak at 2524 cm^{-1}, corresponding to the S−H stretching vibration mode, appears in part d of Figure 3, whereas it disappears in parts a and b of Figure 3. This result strongly suggests that the GSH molecules are anchored on the surface of the silver particles through the sulfur atom of

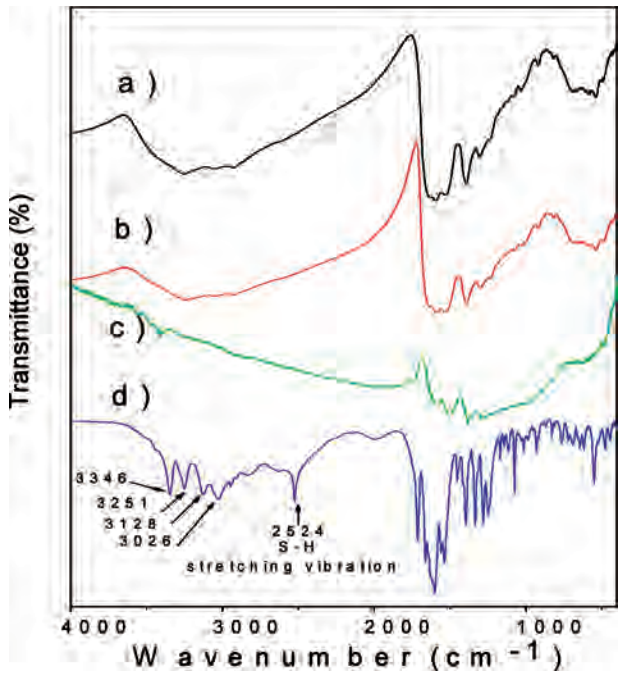

Figure 3. FTIR spectra of GSH and Ag NPs synthesized at different GSH/$AgNO_3$ molar ratio; a) GSH/$AgNO_3$ molar ratio at 1:1, b) GSH/$AgNO_3$ molar ratio at 1:2, c) GSH/$AgNO_3$ molar ratio at 1:10, d) pure GSH.

the mercapto group.[21] The sharp bands peaked at 3346, 3251, 3128, and 3026 cm^{-1} shown in part d of Figure 3 belong to N−H stretching vibration and are observed as three weaker broadening peaks centered at 3255, 3043, and 2926 cm^{-1} in part a of Figure 3 at 3242, 3050, 2926 cm^{-1} in part b of Figure 3, respectively. This provides strong evidence for hydrogen bonding interactions between the adjacent GSH molecules.[14,22] Part c of Figure 3 is the FTIR spectrum of the sample prepared with a GSH/$AgNO_3$ molar ratio of 1:10 and displays weaker signatures compared with parts a and b of Figure 3. This suggests a poor adsorption of GSH molecule on the particle surfaces due to the low GSH/$AgNO_3$ molar ratio.

3.2. Binding of Ag NPs and BSA. The Ag NPs with an average particle size of ca. 6 nm (synthesized at GSH/$AgNO_3$ molar ratio of 1:1) are stable in aqueous solutions for more than six months when it is stored in the dark at room temperature. The good water solubility is shown by the formation of the transparent aqueous solution when the as-synthesized Ag NPs are dispersed in water (the digital photo of the transparent Ag NPs solution shown as Figure S1 in the Supporting Information), which is derived from the hydrophilic biomolecule (glutathione) coating and the nanoscale diameter (6−11 nm). Ag NPs are also ready to bind with the model molecule BSA via the glutaraldehyde linker. Two aldehyde groups of glutaraldehyde react with the amino group of GSH absorbed on the Ag NPs surfaces and the lysine moieties on BSA molecules, respectively, to form covalent linkage.[18] The schematic diagram of the binding procedure between the Ag NPs and BSA molecules is shown as part a of Figure 4 and the assembly was assessed using the SDS-PAGE (sodium dodecylsulfate polyacrylamide gel electrophoresis) technique. The gel electrophoresis has been widely utilized to characterize the conjugation of NPs and biomolecules.[18,23–25] As shown in part b of Figure 4, the electrophoretic results show that Ag NPs (channel 1) traveled faster than the ensembles, even ahead of the electrophoretic front of bromophenol blue. Two independent bands shown in channel 3 representing the Ag NPs and BSA, respectively, suggest that the conjugation did not occur in the absence of glutaraldehyde linker, whereas either Ag NPs or BSA alone formed the oligomers in the presence of linker (channel 2 and channel 10, respectively). The dispersed bands shown in channel 10 traveled slower than BSA alone (channel 11) due to the formation of the BSA oligomers. Bands near the edge of the sample loading are ascribed to the oligomers, which can be minimized through optimizing the reaction conditions such as reaction temperature and reagent ratios.[18] In a primary experiment, a different amount of Ag NPs (0.4, 0.6, 0.8, and 1.0 mg/mL responding to channel 4, 5, 6, and 7, respectively) was employed for the binding procedure with the same amount of BSA and glutaraldehyde linker, and the results show that the larger assembly was not formed in the presence of excess Ag NPs, implying the binding between Ag NPs and proteins is a stoichiometric manner. The obviously weakened bands of Ag NPs ahead of the dye frontier compared with channel 1 and longer tailed bands of BSA compared with channel 10 strongly suggest the successful conjugation between Ag NPs and BSA via a glutaraldehyde linker. Longer denatured times of 3 and 6 min (channels 8 and 9, respectively) compared with 1.5 min (channel 5) at 98 °C prior to electrophoretic separation were employed to assess the thermostability of the ensembles. The similar dispersed bands show a relative resistance of the ensembles to the high temperature. Therefore, the results shown in part b of Figure 4 adequately demonstrate the conjugation of Ag NPs and BSA.

It is well-known that the plasmon resonance of noble metal NPs is strongly dependent on their size, shape, and surface chemistry.[7] In the present study, the size-dependent shift of the surface plasmon resonance positions from ca. 378 to 395 nm was observed when the particle size was changed from 6 to 11 nm (Figure S2 in the Supporting Information), which is probably derived from the quantum size effect. The UV−vis absorption spectra of the Ag NPs and the ensembles of Ag NPs and protein (corresponding to channels 1 and 5 in part b of Figure 3) are shown in part c of Figure 4. The plasmon band at 378 nm is observed in the absorption spectrum of both the Ag NPs [part c (i) in Figure 4] and the ensembles between the Ag NPs and BSA via the glutaraldehyde linker [part c (ii) in Figure 4]. The peak at approximately 220 nm is due to the strong absorption from the Ag NPs, cuvettes, and the water. This peak is not real and is due to the absorbance reaching a maximum value in the UV−vis absorption spectrometer. The inset in the top

(21) Chen, S. H.; Yao, H. S.; Kimura, K. S. *Langmuir* **2001**, *17*, 733.
(22) Tan, Y. W.; Jiang, L.; Li, Y. F.; Zhu, D. B. *J. Phys. Chem. B* **2002**, *106*, 3131.
(23) Zheng, M.; Huang, X. Y. *J. Am. Chem. Soc.* **2004**, *126*, 12047.
(24) Scott, D.; Toney, M.; Muzikár, M. *J. Am. Chem. Soc.* **2008**, *130*, 865.
(25) Tortiglione, C.; Quarta, A.; Tino, A.; Manna, L.; Cingolani, R.; Pellegrino, T. *Bioconjugate Chem.* **2007**, *18*, 829.

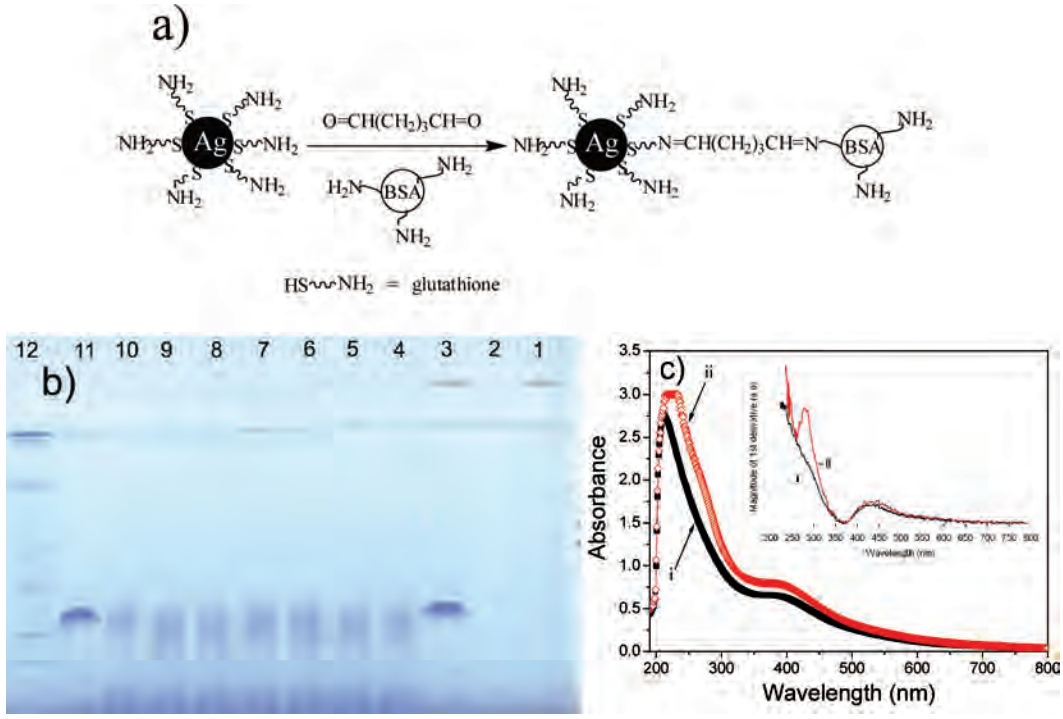

Figure 4. Schematic diagram, SDS-PAGE assay and the UV−vis spectra of Ag NPs binding with BSA molecules via glutaraldehyde linker; a) schematic diagram of the binding procedure between the Ag NPs and BSA molecules via glutaraldehyde linker, b) results of the SDS-PAGE assay: Channel 1: Ag NPs (0.6 mg/mL); channel 2: Ag NPs (0.6 mg/mL) + glutaraldehyde; channel 3: Ag NPs (0.6 mg/mL) + BSA; channel 4: Ag NPs (0.4 mg/mL) + glutaraldehyde + BSA; channels 5, 8, and 9: Ag NPs (0.6 mg/mL) + glutaraldehyde + BSA, samples were denatured for 1.5, 3, and 6 min at 98 °C prior to electrophoresis, respectively; channel 6: Ag NPs (0.8 mg/mL) + glutaraldehyde + BSA; channel 7: Ag NPs (1.0 mg/mL) + glutaraldehyde + BSA; channel 10: BSA + glutaraldehyde; channel 11: BSA; channel 12: the standard protein ladder; c) UV−vis spectra of (i) Ag NPs and (ii) the ensembles between Ag NPs and BSA via glutaraldehyde linker, corresponding to channels 1 and 5 in part b of Figure 3. The top right inset shows the magnitude of the first derivative of the absorption spectra in part c of Figure 3, (i) Ag NPs, and (ii) the ensembles between Ag NPs and BSA via glutaraldehyde linker.

right of part c of Figure 4 shows the magnitude of the first derivative of the respective absorption spectra, taken for 230−800 nm. The derivative of the absorption spectrum is more sensitive to fine changes and reveals the presence of a new feature at 283 nm for the ensembles between Ag NPs and BSA. This feature at 283 nm is attributed to the presence of the glutaraldehyde and BSA attached to Ag NPs. Few obvious changes have been observed in the UV−vis spectra of the mixture of Ag NPs and BSA in the absence of glutaraldehyde linker [part (c) of Figure S3 in the Supporting Information], as well as the mixture of Ag NPs and glutaraldehyde linker [part (b) of Figure S3 in the Supporting Information], compared with that of Ag NPs alone [part (a) of Figure S3 in the Supporting Information]. The feature absorbance of the protein (BSA) at 280 nm [part (f) of Figure S3 in the Supporting Information] is shifted to ca. 272 nm when BSA was mixed with the glutaraldehyde linker [part (e) of Figure S3 in the Supporting Information]. The maximal spectra change is observed in the mixture of Ag NPs and BSA in the presence of a glutaraldehyde linker [part (d) of Figure S3 in the Supporting Information], strongly demonstrating the conjugation between Ag NPs and BSA via the glutaraldehyde linker.

3.3. Anticancer Activities of Ag NPs. To assess the anticancer activity of Ag NPs (the average particle size of ca. 6 nm), the chronic myeloid leukemia cell line (K562 cell) was used as an in vitro cell model. The suppression of K562 cell proliferations by Ag NPs was measured by a MTT (thiazolyl blue) assay, and the results are shown in Figure 5. After K562 cells were incubated with Ag NPs for 6 h, a dose-dependent decrease of cell viability from 94.0 to 81.4% compared with the control was observed while increasing the Ag NPs concentration from 5 to 25 μg/mL (part a of Figure 5). Also, the time-dependent decreases of cell viability can be observed in parts b and c of Figure 5: changing the Ag NPs concentration from 5 to 25 μg/mL, the cell viability decreased from 86.9 to 79.8% compared with the control when the incubation time was 12 h (part b of Figure 5). The viability further decreased from 79.9 to 66.8% compared with the control when the incubation time was prolonged to 24 h (part c of Figure 5). GSH can react with several heavy metals via complexation reaction, which can reduce the metal toxicity to cells.[26] In the present study, the suppression of the K562 cell proliferation caused by GSH was significantly lower than that caused by Ag NPs, strongly suggesting that Ag NPs can effectively suppress the K562 cell proliferations.

We also determined the apoptosis induced by Ag NPs or GSH using the fluorescent microscope and flow cytometer. Only a few apoptotic cells can be observed under the fluorescent microscope when cells were incubated with Ag NPs or GSH at 25 μg/mL concentration for more than 12 h (the fluorescent images shown as Figure S4−S6 in the

(26) Singhal, R. K.; Anderson, M. E.; Meister, A. *FASEB J.* **1987**, *1*, 220.

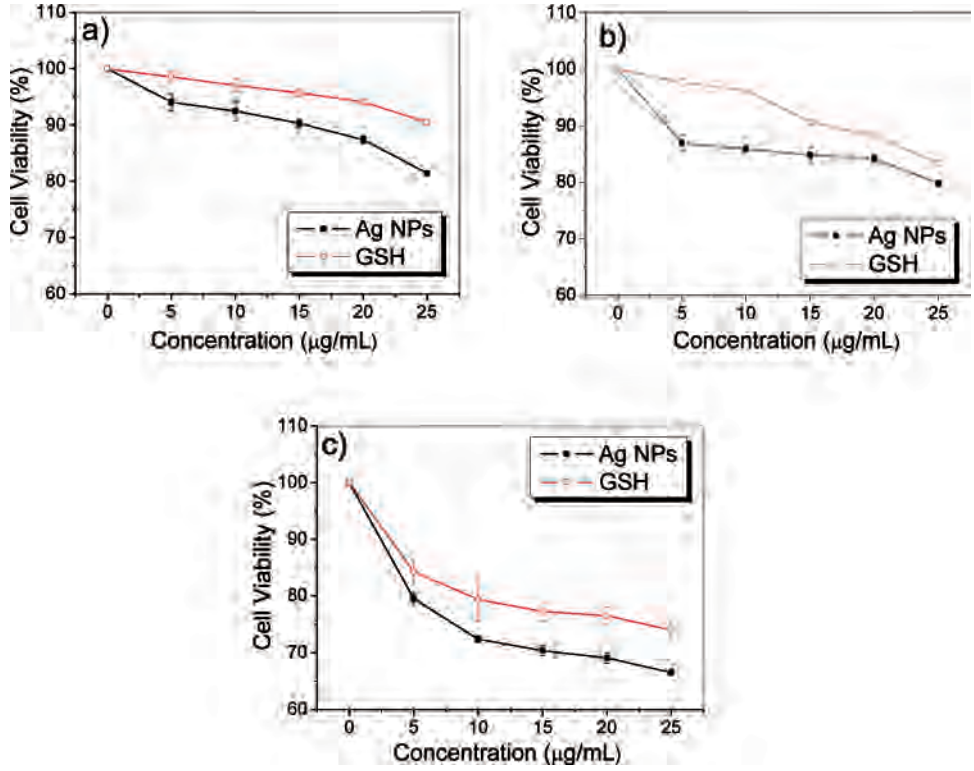

Figure 5. Effects of Ag NPs and GSH on cell viability of human leukemic K562 cells ($n = 5$). a) cell viability of human leukemic K562 cells treated with different concentrations of Ag NPs and GSH for 6 h, b) cell viability of human leukemic K562 cells treated with different concentrations of Ag NPs and GSH for 12 h, and c) cell viability of human leukemic K562 cells treated with different concentrations of Ag NPs and GSH for 24 h.

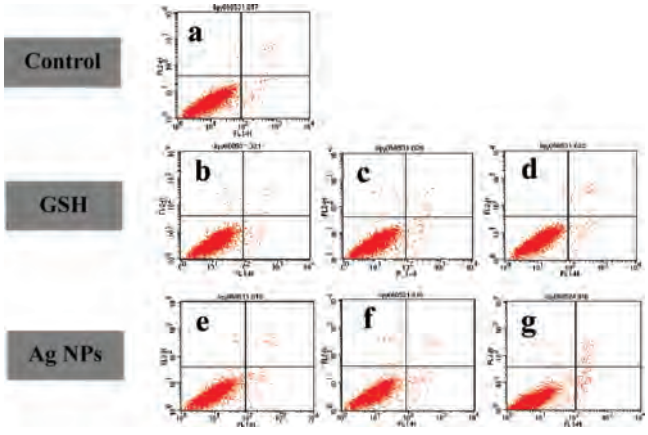

Figure 6. Flow cytometer analysis of K562 cells treated with Ag NPs or GSH for 6 h and then double-labelled with FITC-linked Annexin V/PI. Dual-parameter dot plot of FITC-annexin V fluorescence (x axis, FL1-H) vs PI fluorescence (y axis, FL2-H) shows logarithmic intensity. Quadrants: lower left (FITC-annexin V^-/PI^-) — viable cells; lower right (FITC-annexin V^+/PI^-) — early apoptotic cells; upper right (FITC-annexin V^+/PI^+) — necrotic or late apoptotic cells; upper left (FITC-annexin V^-/PI^+) — damaged cells. a) control; b)−d) cells treated with GSH at 5, 15, and 25 μg/mL for 6 h, respectively; e)−g) cells treated with Ag NPs at 5, 15, and 25 μg/mL for 6 h, respectively.

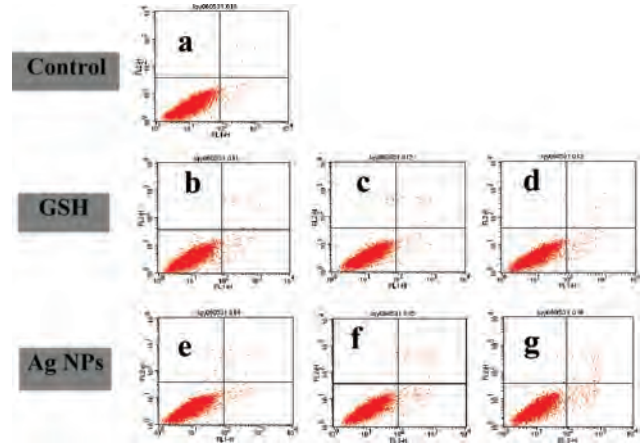

Figure 7. Flow cytometer analysis of K562 cells treated with Ag NPs or GSH for 12 h, and then double-labelled with FITC-linked Annexin V/PI. Dual-parameter dot plot of FITC-annexin V fluorescence (x axis, FL1-H) vs PI fluorescence (y axis, FL2-H) shows logarithmic intensity. Quadrants: lower left (FITC-annexin V^-/PI^-) — viable cells; lower right (FITC-annexin V^+/PI^-) — early apoptotic cells; upper right (FITC-annexin V^+/PI^+) — necrotic or late apoptotic cells; upper left (FITC-annexin V^-/PI^+) — damaged cells. a) control; b)−d) cells treated with GSH at 5, 15, and 25 μg/mL for 12 h, respectively; e)−g) cells treated with Ag NPs at 5, 15, and 25 μg/mL for 12 h, respectively.

Supporting Information). These results were further confirmed by flow cytometer analysis. When K562 cells were incubated with GSH or Ag NPs at concentrations of 5, 15, and 25 μg/mL for 6 h, the percentages of early apoptotic cells were 1.09, 1.19, and 1.76% for GSH and 1.43, 1.44, and 2.17% for Ag NPs, respectively (Figure 6). The percentage of apoptotic cells in the control group was 1.21%. When the incubation time was prolonged to 12 or 24 h, a slight increase of the percentages of apoptotic cells was observed in GSH- and Ag NPs-treated groups (Figures 7 and 8). These results suggest that both Ag NPs and GSH only induced slight apoptosis or necrosis of K562 cells, in agreement with the observation from fluorescence microscopy.

Recently, it was reported that Ag NPs with an average diameter of 15 and 100 nm exhibited cytotoxicity to the rat-liver-derived cell line (BRL 3A cells) through oxidative

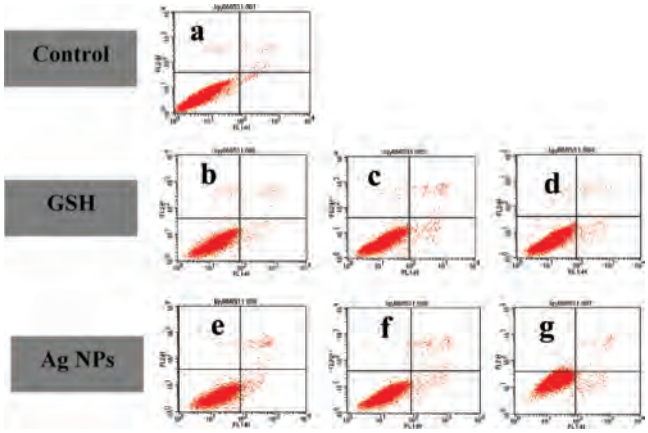

Figure 8. Flow cytometer analysis of K562 cells treated with Ag NPs or GSH for 24 h, and then double-labelled with FITC-linked Annexin V/PI. Dual-parameter dot plot of FITC-annexin V fluorescence (*x* axis, FL1-H) vs PI fluorescence (*y* axis, FL2-H) shows logarithmic intensity. Quadrants: lower left (FITC-annexin V^-/PI^-) — viable cells; lower right (FITC-annexin V^+/PI^-) — early apoptotic cells; upper right (FITC-annexin V^+/PI^+) — necrotic or late apoptotic cells; upper left (FITC-annexin V^-/PI^+) — damaged cells. a) control; b)−d) cells treated with GSH at 5, 15, and 25 μg/mL for 24 h, respectively; e)−g) cells treated with Ag NPs at 5, 15, and 25 μg/mL for 24 h, respectively.

stress, induced significant depletion of the GSH level, decreased the mitochondrial membrane potential, and increased the cellular reactive oxygen species (ROS) level.[27a] The authors also found that Ag NPs at ca. 15 nm in diameter were cytotoxic to the mouse spermatogonial stem cell line (C18−4 cell line), which drastically reduced mitochondrial function and increased membrane leakage.[27b] In our investigations, the percentage of apoptotic or necrotic cells caused by Ag NPs is far lower than the decrease of cell viability. This result implies that the suppression of K562 cell proliferations by Ag NPs was not through the apoptosis or necrosis pathway, whereas the other pathway(s) related to ROS formation may be involved.[28–30] It is noticeable that gold nanospheres, with a variety of surface modifiers at average diameters of ca. 4, 12, and 18 nm, respectively, could be taken up into K562 cells in the lack of detectable cytotoxicity.[31] Therefore, the detailed mechanism about the suppression of K562 cell proliferations by Ag NPs needs to be further investigated, including the comparison with the known drugs and the noncancerous cells.

4. Conclusions

In summary, we presented the synthesis and primary biomedical applications of size-tunable and water-soluble Ag NPs. The Ag NPs at ca. 6 nm in diameter were stable in aqueous solution and were ready to covalently bind with other functional molecules. The optical properties of the Ag NPs were extremely sensitive to the particle size and surface modification. Furthermore, the anticancer potential of Ag NPs was assessed in vitro using human leukemic K562 cells as the cell model. Although the detailed mechanism is not clear, Ag NPs indeed exert an effective suppression to the proliferation of K562 cells. These results suggest a promising perspective of the biomolecule-capped Ag NPs in biomedical fields, especially as a potential clinic drug for cancer therapy.

Acknowledgment. This work was supported by the Program for New Century Excellent Talents in the University of the Education Ministry of China (NCET-04-0066), the project of the Foundation for the Author of National Excellent Doctoral Dissertations (200321), the Program for Key Talents in Tsinghua University (2006), the project of Natural Science Foundation of China (grant 20671056, grant 30572341) and the China Scholarship Council.

Supporting Information Available: The digital photo and UV−vis spectra of silver NPs, fluorescent images of K562 cells treated with Ag NPs. This material is available free of charge via the Internet at http://pubs.acs.org.

IC8002228

(27) (a) Hussain, S. M.; Hess, K. L.; Gearhart, J. M.; Geiss, K. T.; Schlager, J. J. *Toxicol. in Vitro* **2005**, *19*, 975. (b) Braydich-Stolle, L.; Hussain, S.; Schlager, J. J.; Hofmann, M. C. *Toxicol. Sci.* **2005**, *88*, 412.
(28) Brown, J. M.; Attardi, L. D. *Nat. Rev. Cancer* **2005**, *5*, 231.
(29) Yoshimaru, T.; Suzuki, Y.; Inoue, T.; Niide, O.; Ra, C. *Free Radic. Biol. Med.* **2006**, *40*, 1949.
(30) Lovrić, J.; Cho, S. J.; Winnik, F. M.; Maysinger, D. *Chem. Biol.* **2005**, *12*, 1227.
(31) Connor, E. E.; Mwamuka, J.; Gole, A.; Murphy, C. J.; Wyatt, M. D. *Small* **2005**, *1*, 325.